Rayleigh-Bénard Convection in Large-Aspect-Ratio Domains

M. R. Paul,* K-H. Chiam, and M. C. Cross
Department of Physics, California Institute of Technology 114-36, Pasadena, California 91125

P. F. Fischer
Mathematics and Computer Science Division, Argonne National Laboratory, Argonne, Illinois 60439
(Dated: December 5, 2003)

The coarsening and wavenumber selection of striped states growing from random initial conditions are studied in a non-relaxational, spatially extended, and far-from-equilibrium system by performing large-scale numerical simulations of Rayleigh-Bénard convection in a large-aspect-ratio cylindrical domain with experimentally realistic boundaries. We find evidence that various measures of the coarsening dynamics scale in time with different power-law exponents, indicating that multiple length scales are required in describing the time dependent pattern evolution. The translational correlation length scales with time as $t^{0.12}$, the orientational correlation length scales as $t^{0.54}$, and the density of defects scale as $t^{-0.45}$. The final pattern evolves toward the wavenumber where isolated dislocations become motionless, suggesting a possible wavenumber selection mechanism for large-aspect-ratio convection.

PACS numbers: 47.54.+r,47.52.+j,47.20.Bp,47.27.Te

I. INTRODUCTION

Rayleigh-Bénard convection in large-aspect-ratio domains is a canonical system in which to study the emergence of order from initial disorder in a spatially extended system that is driven far-from-equilibrium [1]. A complete understanding of the transient dynamics of the emerging order and the long-time selected pattern is still lacking. In this Letter we investigate the emergence of striped states when a convection layer is quenched into an ordered state from random initial conditions. Although much has been learned for systems of stripes approaching an equilibrium state (relaxational dynamics), much remains unclear for driven systems that are approaching a steady non-equilibrium state (non-relaxational dynamics). This is our focus here.

An important physical property of the final selected pattern is the spatial wavenumber of the convection rolls. For relaxational systems the long-time asymptotic state is the one that minimizes the free energy of the system (or a frozen disordered state if the optimal state is energetically difficult to reach). For non-relaxational systems however, the long-time asymptotic state is not one minimizing a free energy, hence raising the issue of wavenumber selection. Many wavenumber selection mechanisms have been identified for highly controlled situations, often limiting the type and number of pattern defects that interact (for example, selection by grain boundaries, dislocations, or regions of large curvature) or for particular pattern geometries (such as axisymmetric convection or spatial ramps in plate separation) [2–4]. However, an understanding of the wavenumber selected in a large-aspect-ratio domain initiated from small random thermal perturbations remains elusive. Therefore, in a non-relaxational system such as convection, the long-time asymptotic state is unknown *a priori* and can be one of an infinite number of ordered states. The effect on the coarsening dynamics is not currently understood and is discussed further below.

Substantial work has been done on the pattern coarsening in relaxational systems that occurs as domains of uniform stripes compete and grow in size. In this case, the dynamics can be understood in terms of the monotonic decrease of the free energy. This provides a useful tool to look for important dynamical interactions and has been exploited for the case of diblock copolymers [5]. Experiments using diblock copolymers have been performed in extremely-large-aspect ratios with more than 10^5 microdomain repeat spacings, effectively eliminating boundary effects, and for durations long enough to reach striped states free of defects. The orientational correlation length, ξ_o, was found to grow in time as $\xi_o \sim t^{1/4}$, and the dominant coarsening mechanism was determined to be annihilation events involving disclination quadrupoles.

The Swift-Hohenberg equation (SH), which is relaxational, and the Generalized Swift-Hohenberg equation (GSH), which can be either relaxational or non-relaxational depending on the choice of the nonlinearity, have been studied as model systems for the coarsening of striped patterns in periodic geometries. For the SH equation a measure of the translational correlation length, ξ_T, was found to vary as $t^{1/5}$ in the absence of noise and as $t^{1/4}$ in the presence of noise [6], although recent deterministic simulations performed close to threshold in the absence of noise give $t^{1/3}$ [7]. A study of the SH equation and a non-relaxational GSH equation found that the domain size scaled as $t^{1/5}$ in all cases [8]. However, the non-relaxational results gave an orientational length scale given by $\xi_o \sim t^{1/2}$, and the stripe patterns were found

*Electronic address: mpaul@caltech.edu

to evolve toward a final wavenumber, q_d, where isolated dislocations become stationary.

To date, experiments on the coarsening dynamics of a far-from-equilibrium, spatially extended non-relaxational system have been performed only for the electroconvection of a liquid nematic crystal [9]. Here the pattern is asymmetric, with convection rolls forming zig and zag rolls at an angle $\pm\theta$ relative to the nematic anisotropy direction. For this system, using isotropic measures of the domain growth, it has been found that the domains grow as $t^{1/5}$ and the domain wall length grows as $t^{1/4}$ [9].

Coarsening experiments on Rayleigh-Bénard convection in a large-aspect-ratio container have not been conducted. A considerable experimental difficulty is in achieving a spatially uniform initial state composed of random perturbations; slight variations in the apparatus will influence the initial pattern emerging from the disorder. Numerical simulations are free of these difficulties, however, allowing us to investigate the coarsening dynamics of Rayleigh-Bénard convection in an experimentally realistic geometry for the first time.

II. DISCUSSION

We study numerically, using a parallel spectral element code [10], Rayleigh-Bénard convection in a large-aspect-ratio cylindrical domain (see [11] for related applications). The aspect ratio is a measure of the spatial extent of the system and for a cylindrical geometry is defined as $\Gamma = r/d$, where r is the radius of the convection cell and d is the depth. The Boussinesq equations that govern the dynamics of the velocity $\vec{u}$, temperature T, and pressure p, fields are,

$$\begin{aligned} \sigma^{-1}\left(\partial_t + \vec{u}\bullet\vec{\nabla}\right)\vec{u} &= -\vec{\nabla}p + RT\hat{z} + \nabla^2\vec{u}, \\ \left(\partial_t + \vec{u}\bullet\vec{\nabla}\right)T &= \nabla^2 T, \\ \vec{\nabla}\bullet\vec{u} &= 0, \end{aligned}$$

where time differentiation is given by ∂_t, $\hat{z}$ is a unit vector in the vertical direction, σ is the Prandtl number, and R is the Rayleigh number. The equations are nondimensionalized using the layer depth d, the vertical diffusion time for heat τ_v, and the constant temperature difference across the layer ΔT, as the length, time, and temperature scales, respectively. All bounding surfaces are no slip, the lower and upper surfaces ($z = 0, 1$) are held at constant temperature, and the sidewalls are perfectly insulating.

We study the pattern evolution from small random thermal perturbations, $\delta T \sim 0.01$, in a large-aspect-ratio domain, $\Gamma = 57$, containing a fluid with $\sigma = 1.4$. We present results for two simulations at $\epsilon = 0.27$ (where $\epsilon = (R - R_c)/R_c$ is the reduced Rayleigh number and R_c is the critical Rayleigh number) that differ only in the particular choice of random initial conditions. Figure 1 illustrates the time evolution of the temperature field at mid-depth for these parameters. At early times

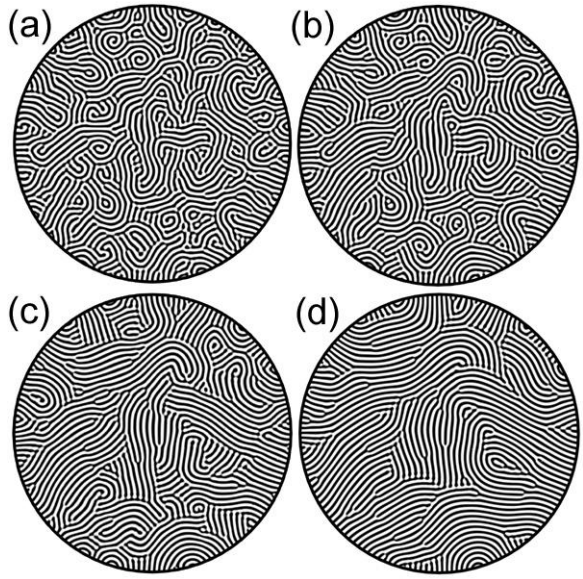

FIG. 1: The mid-depth temperature field, T, at times $t = 16, 32, 64$ and 128, panels (a)-(d), repsectively. Light regions indicate warm rising fluid, and dark regions indicate cool descending fluid. Simulations parameters: $\epsilon = 0.27$, $\Gamma = 57$, and $\sigma = 1.4$.

(see Fig. 1(a)) there are present many small patches of arbitrarily oriented rolls, as well as many defects, including disclinations, dislocations, grain boundaries, spirals, wall foci, and targets. As time progresses, the pattern coarsens into larger domains of stripes with fewer defects mostly dominated by wall foci, grain boundaries, and isolated dislocations.

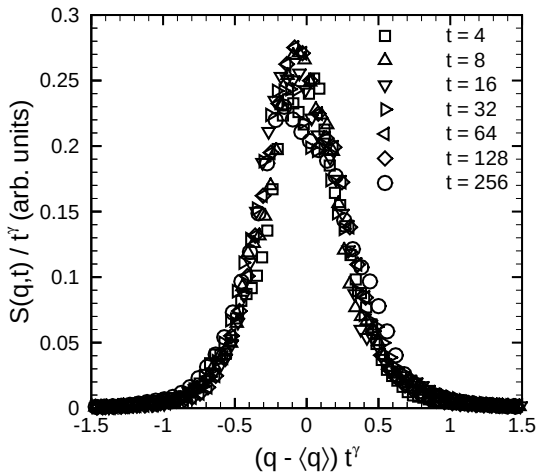

FIG. 2: The scaling property of the azimuthally averaged structure factor $S(q,t)$ is illustrated by the data collapse found at various times when plotting $S(q,t)/t^\gamma$ versus $(q - \langle q\rangle)t^\gamma$ with $\gamma = 0.12$.

A measure of the translational order is the translational correlation length, ξ_T, which is calculated from the time variation of the second moment of the azimuthally averaged structure factor $S(q,t)$. The structure factor is the square of the modulus of the spatial Fourier transform of the temperature perturbation field at mid-depth. The scaling property of $S(q,t)$ is illustrated in Fig. 2 by the data collapse at various times by plotting $S(q,t)/t^{\gamma}$ versus $(q-\langle q\rangle)t^{\gamma}$ for $\gamma = 0.12$ (where $\langle q\rangle$ is the average wavenumber). The data collapse occurs over a range of $4 \lesssim t \lesssim 256$ indicating a window of time over which the scaling Ansatz is valid. For large times $t > 256$, the scaling breakdown indicates the influence of lateral boundaries and finite size effects. As shown in Fig. 2, the collapse of the $S(q,t)$ curves at early time $t = 4$ (squares) and late time $t = 256$ (circles) are beginning to show some deviation. In the discussion that follows, we consider the dynamics only in the scaling regime. The translational correlation length is shown in Fig. 3(a). The scaling of $\xi_T \sim t^{0.12}$ indicates very slow growth when compared with the predominance of $t^{1/4}$ and $t^{1/5}$ scalings found in a variety of other systems as already discussed. Similar results are obtained from measuring the time variation of the inverse half-width at half-height of $S(q,t)$.

The time dependence of local orientational order is measured from the time variation of the orientational correlation length, ξ_o. This is determined by calculating the second moment of the azimuthally averaged Fourier intensity of $\mathrm{Re}[e^{2i\theta}]$, where θ is the local angle of the stripes [12]. As shown in Fig. 3(b), $\xi_o \sim t^{0.54}$, which grows faster than ξ_T, as shown by the long dashed line, suggesting the presence of an additional length scale in the coarsening dynamics.

The spatial distribution of defects is quantified in Fig. 4 by highlighting regions of large local curvature, κ, where $\kappa = \vec{\nabla}\bullet\hat{k}$ ($\hat{k} = \vec{k}/|k|$ is the local unit wavevector [12]). There are many defects early in the time evolution; however, as time progresses, most of the defects are annihilated, leaving domain walls and isolated dislocations. A defect density, ρ_d, can be defined as the ratio of the total area covered by defects. The time evolution of ρ_d is shown in Fig. 5 and exhibits a scaling of $\rho_d \sim t^{-0.45}$. For a pattern dominated by isolated defects exhibiting isotropic growth in all directions, which is approximately valid for the very early time evolution ($t \lesssim 10$), this suggests a scaling of the domain size as $\xi_d \sim t^{0.23}$. On the other hand, for patterns composed of defect lines (or grain boundaries) of unit width, which is relevant for later times ($t \gtrsim 10$), ρ_d is the length of the line suggesting a scaling of $\xi_d \sim t^{0.45}$.

The long-time asymptotic state of a convection pattern free of the influence of lateral boundaries remains poorly understood. Our results suggest that the pattern evolves toward the wavenumber where isolated dislocations become motionless, q_d (see Fig. 6). The values of q_d have been obtained, for the fluid parameters of interest here, both experimentally and numerically by measuring

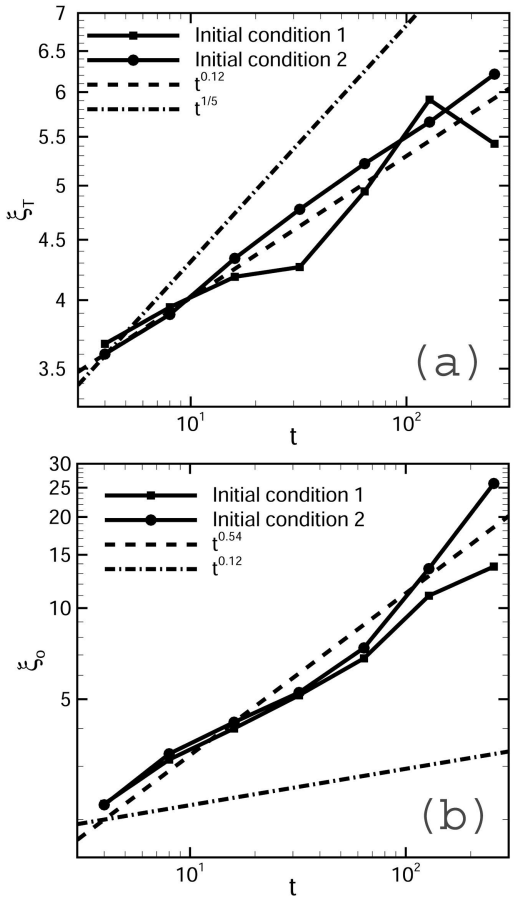

FIG. 3: Panel (a): The translational correlation length ξ_T as a function of time. The dashed line is a power-law fit yielding a scaling of $t^{0.12}$. The dash-dotted line illustrates a scaling of $t^{1/5}$ for reference. Panel (b): The orientational correlation length ξ_o as a function of time. The dashed line is a power-law fit yielding a scaling of $t^{0.54}$. For reference the dashed-dotted line shows the time variation of $\xi_T \sim t^{0.12}$ from panel (a) to illustrate the two different length scales.

the climb velocity of a dislocation in a background of either straight parallel rolls or a giant one-armed spiral and interpolating to find the wavenumber of zero climb velocity [13]. For reference, the wavenumber selected by patches of curved rolls or foci, q_f, is also shown [14]. The wavenumber q_f is also where $D_{\perp} \to 0$ in the absence of mean flow ($D_{\perp}$ is the diffusion coefficient perpendicular to the wavevector in the Pomeau-Manville phase equation [15]). For large times where the effects of the boundaries are important $256 \lesssim t \lesssim 500$ we find a slow increase in the wavenumber indicating that q_f may be selected for at very long times by the prevalence of curved rolls from large wall foci. In a similar calculation for slightly more supercritical conditions, $\epsilon = 0.46$, the pattern wavenumber evolves, for times in the scaling regime, to $q = 2.58$ where $q_d = 2.63$, and $q_f = 3.09$, again suggesting a selected wavenumber of q_d. These results indicate that the

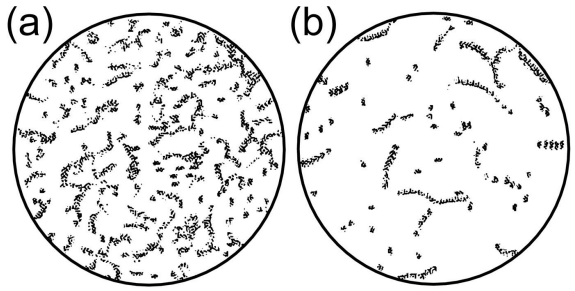

FIG. 4: Contour plots illustrating the spatial distribution of defects: panel (a) $t = 16$, panel (b) $t = 128$. Defect regions are black, and defect-free regions are white. The ratio of the defect containing area to the total area yields a measure of the defect density ρ_d, which is shown as a function of time in Fig. 5. The patterns corresponding to these defect distributions are displayed in Fig. 1(a) and (d).

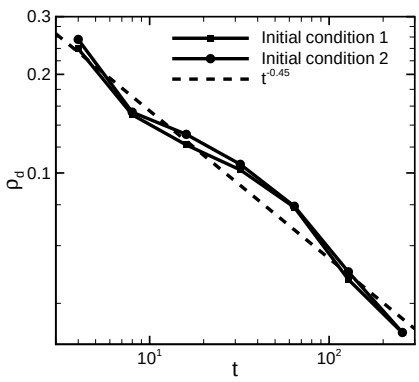

FIG. 5: The defect density, ρ_d, as a function of time. A power-law fit to the data is shown by the dashed line with $\xi_d \sim t^{-0.45}$.

wavenumber selected in large-aspect-ratio domains is q_d in agreement with the predictions made from numerical simulations of the GSH equations [8].

III. CONCLUSION

We have investigated domain coarsening and wavenumber selection in a non-relaxational, extended, and far-from-equilibrium system by performing full numerical simulations of Rayleigh-Bénard convection with experimentally realistic boundary conditions. In non-relaxational systems the long-time asymptotic state is unknown, thus raising the question of wavenumber selection and the issue of how this might affect the coarsening dynamics. For Rayleigh-Bénard convection we find that multiple length scales are necessary to describe the pattern evolution in time. The coarsening dynamics involve the complicated evolution of many

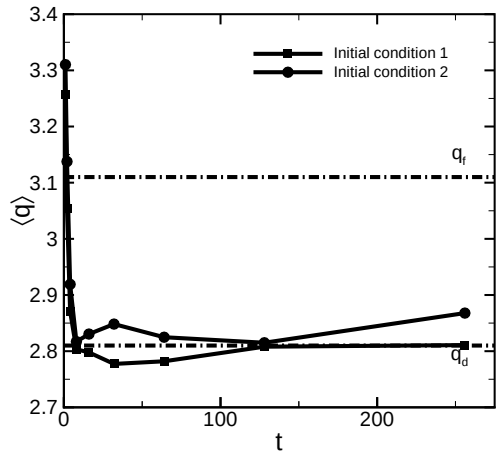

FIG. 6: Wavenumber variation as a function of time. Wavenumber selected by zero velocity dislocations $q_d = 2.81$ [13] and wavenumber selected by patches of curved convection rolls $q_f = 3.11$ [14].

types of defects, making it difficult to identify dominant coarsening mechanisms responsible for the observed scaling exponents. Further insight could be gained by studying defect interactions in simpler prescribed situations. We also find that the pattern selects the wavenumber where isolated dislocations become stationary, suggesting that this may be the wavenumber selected from random initial conditions in the absence of influences from the lateral boundaries.

This research was supported by the U.S. Department of Energy, Grant DE-FT02-98ER14892, and the Mathematical, Information, and Computational Sciences Division subprogram of the Office of Advanced Scientific Computing Research, Office of Science, U.S. Department of Energy, under Contract W-31-109-Eng-38. We also acknowledge the Caltech Center for Advanced Computing Research and the North Carolina Supercomputing Center.

[1] M. C. Cross and P. C. Hohenberg, Rev. of Mod. Phys. **65**, 851 (1993).
[2] I. Catton, J. Heat Trans. **110**, 1154 (1988).
[3] M. C. Cross, P. C. Hohenberg, and S. A. Safran, Physica D **5**, 75 (1982).
[4] M. R. Paul, M. C. Cross, and P. F. Fischer, Phys. Rev. E **66**, 046210 (2002).
[5] C. Harrison, Z. Cheng, S. Sethuraman, D. Huse, P. M.

Chaikin, D. A. Vega, J. M. Sebastian, R. A. Register, and D. H. Adamson, Phys. Rev. E **66**, 011706 (2002).
[6] K. R. Elder, J. Viñals, and M. Grant, Phys. Rev. Lett.. **68**, 3024 (1992).
[7] D. Boyer and Vinals, Phys. Rev. E **64**, 050101 (2001).
[8] M. C. Cross and D. I. Meiron, Phys. Rev. Lett. **75**, 2152 (1995).
[9] L. Purvis and M. Dennin, Phys. Rev. Lett. **86**, 5898 (2001).
[10] P. F. Fischer, J. Comp. Phys. **133**, 84 (1997).
[11] M. R. Paul, K.-H. Chiam, M. C. Cross, P. F. Fischer, and H. S. Greenside, Physica D **184**, 114 (2003).
[12] D. A. Egolf, I. V. Melnikov, and E. Bodenschatz, Phys. Rev. Lett. **80**, 3228 (1998).
[13] B. B. Plapp, D. A. Egolf, E. Bodenschatz, and W. Pesch, Phys. Rev. Lett. **81**, 5334 (1998).
[14] J. C. Buell and I. Catton, Phys. Fluids **29**, 23 (1986).
[15] Y. Pomeau and P. Manneville, J. Physique Lett. **40**, 609 (1979).